Documentation – User's Guide

Polarimetric tools

GAMMA REMOTE SENSING

Version 1.2 – July 2013

Table of contents

List of acronyms

ALOS	*Advanced Land Observing Satellite*
ASAR	*Advanced Synthetic Aperture Radar*
EORC	*Earth Observation Research Center*
ENVISAT	*Environmental Satellite*
ERS	*European Remote Sensing (Satellite)*
ISP	*Interferometric SAR Processor*
JAXA	*Japan Aerospace Exploration Agency*
JERS-1	*Japanese Earth Resources Satellite*
LAT	*Land Application Tools*
MLI	*Multi-look Intensity*
PALSAR	*Phase Array type L-band Synthetic Aperture Radar*
ESA	*European Space Agency*
ISP	*Interferometric SAR Processor*
SAR	*Synthetic Aperture Radar*
SIR	*Shuttle Imaging Radar*
SLC	*Single Look Complex*

1. Introduction

The propagation of an electromagnetic wave through a medium implies that amplitude and phase change in time and space. The vectors describing the transmitted electric and magnetic fields describe a trajectory in the plane of propagation, i.e. on the plane to which the direction of propagation of the wave is perpendicular. If the extreme of the vector describes a line, the wave is said to be linearly polarized. If the extreme of the vector describes a circle or, more in general, an ellipse, the wave is said to be circularly or elliptically polarized. The linear polarization can be seen as a particular case of elliptical polarization. Regardless of the trajectory described, the electric field (and in a similar way the magnetic field) can be represented in form of two components, the horizontal and the vertical component. The reference system used to define the horizontal and the vertical direction is centered along the direction of propagation, with the out-of-plane axis along this direction. In the polarization plane the two axes correspond to the direction parallel to the ground and the direction perpendicular to it. Figure 1 shows the polarization ellipse, i.e. the trajectory describe by the vector of the electric field during the propagation, the reference system and the most relevant parameters used to describe the polarization of a wave. The x-axis corresponds to the horizontal direction. The y-axis corresponds to the vertical direction. The electric field represented by the thickened vector has horizontal component E_x and vertical component E_y. The position of the vector on the plane is defined by the phase, φ. The polarization ellipse, i.e. the trajectory described by the vector of the electric field is characterized by the semi-major and semi-minor axis the ellipticity angle, χ, and the orientation angle, ψ. The ellipticity is defined as the ratio between the semi-minor and semi-major axis.
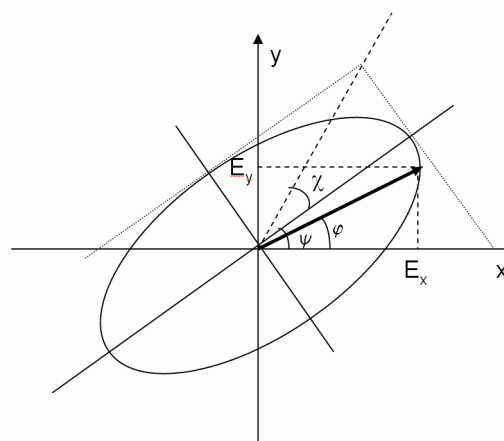
Figure 1. Polarization ellipse.

Figure 1 shows that an e.m. wave can be fully characterized when the two components along the horizontal or vertical axis are known. Limiting our considerations to active microwave systems, at the scattering level variations of the polarization properties of the microwave can occur depending on the objects being viewed by the radar. One of the main advantages of polarimetric techniques is the possibility to separate scattering contributions of different nature. For this purpose the scattering matrix **S** is analyzed with different techniques in order to extract information about the scattering process.

The scattering matrix basically contains the signal received after scattering in two polarizations, one being orthogonal to the other:

$$\mathbf{S} = \begin{bmatrix} S_{xx} & S_{xy} \\ S_{yx} & S_{yy} \end{bmatrix} \tag{1}$$

where S_{xy} are the complex scattering coefficients at xy-pol (SLC data points). In the monostatic case, where receiver and transmitter coincide, the scattering matrix in symmetric, i.e. $S_{xy}=S_{yx}$ so that the entire scattering is defined by three components. Typically it is referred to x as the horizontal direction and v as the vertical direction. The scattering matrix can be represented in other basis in order to better highlight certain mechanisms as mentioned before. This topic will be further addressed in Section 6.

In the monostatic case, i.e. receiver and transmitter coincident, a representation of the scattering information is the 3-D lexicographic feature vector:

$$\underline{\Omega} = \begin{bmatrix} S_{xx} & \sqrt{2}S_{xy} & S_{yy} \end{bmatrix}^T \tag{2}$$

The Pauli decomposition leads to the generation of the "3-D Pauli feature vector"

$$\underline{k} = \frac{1}{\sqrt{2}} \begin{bmatrix} S_{xx} + S_{yy} & S_{xx} - S_{yy} & 2S_{xy} \end{bmatrix}^T \tag{3}$$

This representation allows separating odd, even and the 45° tilted bounce components respectively.

$\text{Pauli1} = S_{hh} + S_{vv}$ odd bounce

$\text{Pauli2} = S_{hh} - S_{vv}$ even bounce   (4)

$\text{Pauli3} = S_{hv} + S_{vh}$ 45° tilted bounce

It is very convenient as a quality check of the polarimetric data.

The total power of either the Pauli feature vector or the lexicographic feature vector corresponds to the span of the scattering matrix, defined as:

$$Span(S) = |S_{xx}|^2 + 2|S_{xy}|^2 + |S_{yy}|^2$$

1.1. Polarimetric spaceborne SAR systems

Depending on the capability of a radar to transmit and/or receive one or both polarization, one speaks of single-, double or full-polarization. Singe-polarization means that the radar sends a signal in one polarization (horizontal or vertical) and receives in the same polarization. This implies that significant part of the scattering information is lost and the scattering matrix reduces to one term from the main diagonal. With specific regard to spaceborne SAR, the early systems (Seasat, ERS, JERS and RADARSAT-1) had all only single polarization capabilities.(see Table 1). Dual-polarization refers to the case when only two of the four elements of the scattering matrix are available (e.g. HH and HV-polarization). Full-

polarization capability is implemented in all recent spaceborne SAR systems (see Table 1). In addition, during the Shuttle SIR-C mission in 1994 several datasets in single, dual- and full-polarization have been acquired.

Table 1. SAR sensors and polarization capabilities.

SAR sensor	Lifespan	Polarization
Seasat	1978 (3 months)	Single (HH)
ERS-1	1991-1999	Single (VV)
ERS-2	1995-2012	Single (VV)
JERS-1	1992-1998	Single (HH)
RADARSAT-1	1995-2013	Single (HH)
ENVISAT ASAR	2002-2012	Single and dual
COSMO-SkyMed	2007-	Single and dual
ALOS PALSAR	2006-2011	Single, dual and full-polarization
TerraSAR-X	2007-	Single, dual and full-polarization
RADARSAT-2	2007-	Single, dual and full-polarization
UAVSAR	-	Single, dual and full-polarization
RISAT-1	2012-	Single, dual and full-polarization

Scope of this manual is to provide the user of the GAMMA software with a description of the polarimetric processing capabilities offered by the software. The LAT module of the GAMMA Software includes a number of general purpose tools and that can be applied to polarimetric processing as well as a number of polarimetry-specific programs. For an overview it is referred to the User's Guide of the LAT module. For specific information on each of the programs that will be presented throughout this manual, it is referred to the Reference Manual of the LAT module. In the following these processing capabilities will be described with a brief theoretical introduction followed by a set of instructions on how to do specific actions using the software.

2. SAR dataset

The polarimetric processing steps described hereafter are applied to a full polarimetric ALOS PALSAR dataset covering the region of Berne, Switzerland (ALPSRP039360940-P1.1__A). The data was obtained from JAXA EORC through PI project 175. The dataset was acquired on 2006-10-20 with a 23 degrees incidence angle. Each image has been obtained in single-look complex format.

The SLC data was first converted to the format of the GAMMA software with the program ***par_EORC_PALSAR*** (part of the ISP module or GEO_only module). With this program an ISP SLC image parameter file has also been obtained. The program is applied separately for each image forming the polarimetric dataset.

```
par_EORC_PALSAR  LED-ALPSRP039360940-P1.1__A  20061020_hh_full.slc.par  IMG-
HH-ALPSRP039360940-P1.1__A 20061020_hh_full.slc
```

```
par_EORC_PALSAR  LED-ALPSRP039360940-P1.1__A  20061020_hv_full.slc.par  IMG-
HV-ALPSRP039360940-P1.1__A 20061020_hv_full.slc
```

```
par_EORC_PALSAR  LED-ALPSRP039360940-P1.1__A  20061020_vh_full.slc.par  IMG-
VH-ALPSRP039360940-P1.1__A 20061020_vh_full.slc
```

```
par_EORC_PALSAR  LED-ALPSRP039360940-P1.1__A  20061020_vv_full.slc.par  IMG-
VV-ALPSRP039360940-P1.1__A 20061020_vv_full.slc
```

For each image the term "full" has been included in the file name to distinguish these images from those that will be used for polarimetric processing, which will correspond to a subset of the full dataset. Each image consists of 1536 range pixels and 18432 azimuth lines, corresponding to approximately 30 km in range and approximately 70 km in azimuth. Each image is in FCOMPLEX, i.e. floating point complex format, this meaning that the each pixel consists of 4 byte for the real and for 4 byte for the imaginary part.

From each image a subset has been extracted consisting of 800 columns and 4200 lines. Part of an SLC can be extracted using the program ***SLC_copy*** (ISP module). The first 800 columns and 4200 lines starting from line 901 have been extracted. The area covered by the subset consists of the region of Berne.

```
SLC_copy   20061020_hh_full.slc   20061020_hh_full.slc.par   20061020.hh.slc0
20061020.hh.slc0.par 1 - 800 901 4200
```

```
SLC_copy   20061020_hv_full.slc   20061020_hv_full.slc.par   20061020.hv.slc0
20061020.hv.slc0.par 1 - 800 901 4200
```

```
SLC_copy   20061020_vh_full.slc   20061020_vh_full.slc.par   20061020.vh.slc0
20061020.vh.slc0.par 1 - 800 901 4200
```

```
SLC_copy   20061020_vv_full.slc   20061020_vv_full.slc.par   20061020.vv.slc0
20061020.vv.slc0.par 1 - 800 901 4200
```

The extension "slc0" is used to indicate that the SLC will still be processed before being used for polarimetric processing. SLC data from JAXA EORC still need to be calibrated using the calibration factor provided by JAXA. For SLC data the calibration factor is equal to -115 dB. It is referred to the homepage of the ALOS PALSAR mission for more details.

For calibration the program ***radcal_SLC*** is used (ISP module).

```
radcal_SLC    20061020.hh.slc0    20061020.hh.slc0.par    20061020.hh.slc
20061020.hh.slc.par 1 - 0 0 0 0 -115.0
```

```
radcal_SLC    20061020.hv.slc0    20061020.hv.slc0.par    20061020.hv.slc
20061020.hv.slc.par 1 - 0 0 0 0 -115.0
```

```
radcal_SLC    20061020.vh.slc0    20061020.vh.slc0.par    20061020.vh.slc
20061020.vh.slc.par 1 - 0 0 0 0 -115.0
```

```
radcal_SLC    20061020.vv.slc0    20061020.vv.slc0.par    20061020.vv.slc
20061020.vv.slc.par 1 - 0 0 0 0 -115.0
```

For the fully calibrated SLCs multi-look intensity images are finally obtained with the program ***multi_look*** (ISP module). For an ALOS PALSAR full-polarimetric dataset suggested multi-look factors are 1 and 7 are respectively for the range and azimuth direction in order to obtain roughly squared pixels (approximately 25 m).

```
multi_look      20061020.hh.slc      20061020.hh.slc.par      20061020.hh.mli
20061020.hh.mli.par 1 7

multi_look      20061020.hv.slc      20061020.hv.slc.par      20061020.hv.mli
20061020.hv.mli.par 1 7

multi_look      20061020.vh.slc      20061020.vh.slc.par      20061020.vh.mli
20061020.vh.mli.par 1 7

multi_look      20061020.vv.slc      20061020.vv.slc.par      20061020.vv.mli
20061020.vv.mli.par 1 7
```

Each image consists of 800 range pixels and 600 lines. Figure 1 shows the intensity of each of the four images forming the dataset.

HH

HV

VV

VH
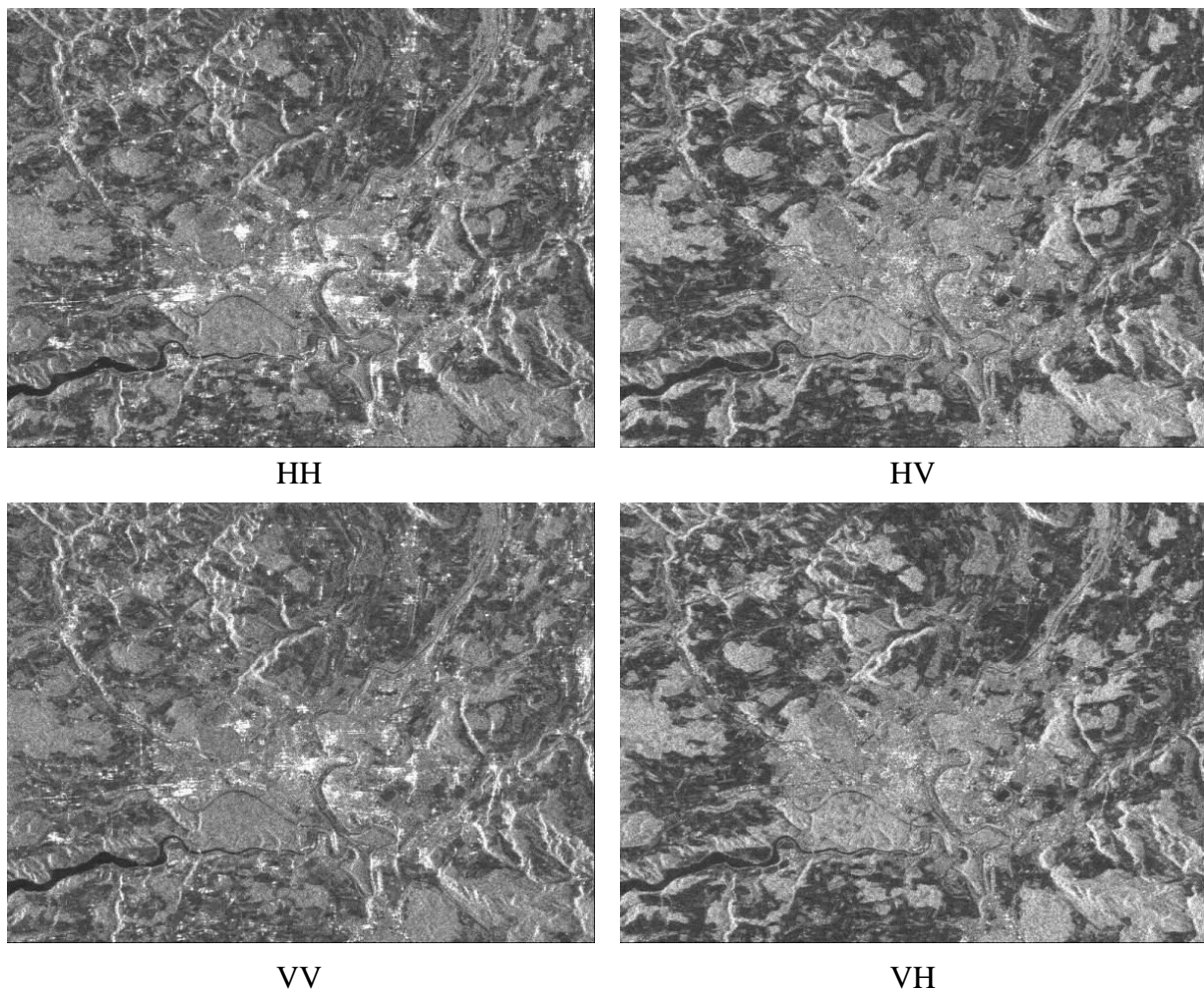
Figure 1. Multi-look intensity HH, HV and VV images.

3. Representation of polarimetric data

Since polarimetric datasets consist of several images, a combination of the individual images into a new quantity or in form of RGB color composites are effective ways for displaying their information content.

3.1. Span

The span of the scattering matrix corresponds to the linear combination of the intensities of the matrix elements. The resulting image corresponds to a filtered version of the individual images, where the effect of the different scatterers on the total backscatter becomes more evident. With the LAT module, the span can be computed starting from the MLIs using the program ***lin_comb*** as follows:

```
lin_comb  3  20061020.hh.mli  20061020.hv.mli  20061020.vv.mli  0  1  2  1
20061020.span 800
```

The image of the span can be displayed with the program of the DISP module ***dispwr*** or ***dis_dB*** if the logarithmic scale is preferred.

```
dispwr 20061020.span 800
```

Figure 2 shows the image of the span. Compared to the MLIs in Figure 1 the span appears less noisy and with clearer details.
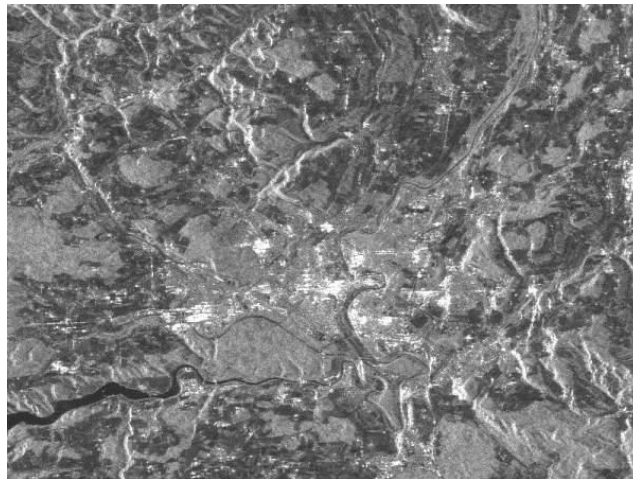
Figure 2. Image of the span of the ALOS PALSAR polarimetric dataset.

3.2. Lexicographic feature vector representation

Another possibility to represent polarimetric images is in the form of color composites. The lexicographic feature vector representation combines HH in red, HV in green and VV in blue.

Figure 3 illustrates the RGB color composite. The city of Berne in the centre of the image appears in pink. So do the chain of towns close to the city. This is due to the strong HH and VV components and the negligible HV component. In urban areas the scattering is primarily related to direct surface scattering and double-bounces, which are predominant in the co-polarized images. Vegetated areas, e.g. forests, appear in green, because of the volume scattering which is predominant in cross-polarization. Finally, the image shows many areas in blue/purple, indicating a strong VV component as well as a significant HH component to the total backscatter. These areas correspond to bare fields, for which surface scattering is the main scattering mechanism.
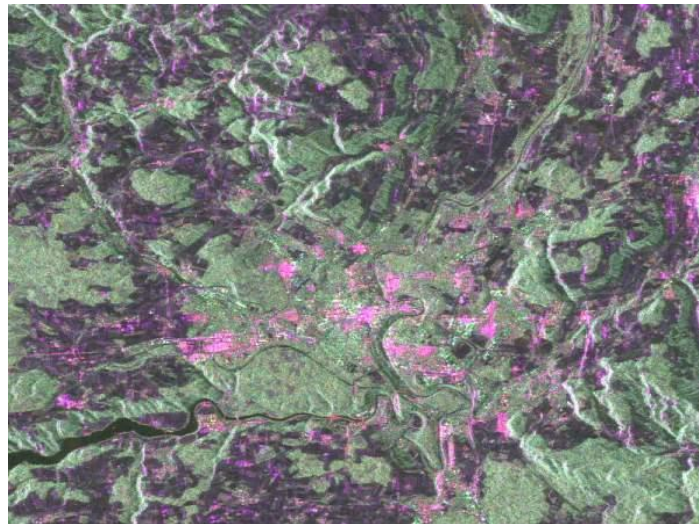
Figure 3. RGB color composite of a full-polarimetric ALOS PALSAR dataset over Berne, Switzerland, in the lexicographic representation (R=HH, B=HV, G=VV).

This RGB can be obtained with the programs of the LAT module as follows:

At first SUNraster (or bmp) images for each channel need to be generated. This can be done with the DISP program *raspwr*. Alternatively the programs *ras_dB* (logarithmic scale) or *ras_linear* (linear scale) can be used. In this example SUNraster images are generated with a file name given by the input file name and extension "ras".

```
raspwr 20061020.hh.mli 800

raspwr 20061020.hv.mli 800

raspwr 20061020.vv.mli 800
```

The RGB color composite is obtained with the program *ras_to_rgb*:

```
ras_to_rgb  20061020.hh.mli.ras  20061020.hv.mli.ras  20061020.vv.mli.ras
20061020.lexic.rgb.ras
```

This image is displayed in Figure 4. With the GAMMA software the RGB image can be displayed with the program *disras*

```
disras 20061020.lexic.rgb.ras
```

3.3. Pauli decomposition and color coding

If the Pauli representation in (4) is adopted, another RGB can be generated. At first we need to generate the individual components of the vector *k*. This can be done with the program *pauli* as follows:

```
pauli 20061020.hh.slc 20061020.vv.slc 20061020.hv.slc 20061020.hh.slc.par
20061020.vv.slc.par 20061020.hv.slc.par 20061020.pauli
```

The vector components have file name "20061020" and extensions "pauli_alpha", "pauli_beta" and "pauli_gamma".

The Pauli RGB color composite consists of the following combination: 2nd component (i.e. difference of co-pol terms, even bounce) in red, 3rd component (i.e. cross-pol term, 45 degrees tilted bounce) in green and 1st component (i.e. sum of co-pol terms, odd bounce) in blue. To generate the RGB with the GAMMA software, at first the SUNraster version of the three Pauli components must be generated. Since the data is in FCOMPLEX format and we are primarily interested in the magnitude, the program *rasSLC* (DISP module) is used. To decrease noise, multi-looking is applied with factors 1 and 7 (see Section 2).

```
rasSLC 20061020.pauli_alpha.slc 800 - - 1 7

rasSLC 20061020.pauli_beta.slc 800 - - 1 7

rasSLC 20061020.pauli_gamma.slc 800 - - 1 7
```

With the program *ras_to_rgb* the RGB can be obtained.

```
ras_to_rgb    20061020.pauli_beta.slc.ras    20061020.pauli_gamma.slc.ras
20061020.pauli_alpha.slc.ras 20061020.pauli.rgb.ras
```

Pauli 1: HH+VV (odd bounce)

Pauli 2: HH-VV (even bounce)

Pauli 3: 2*HV (45 degrees)
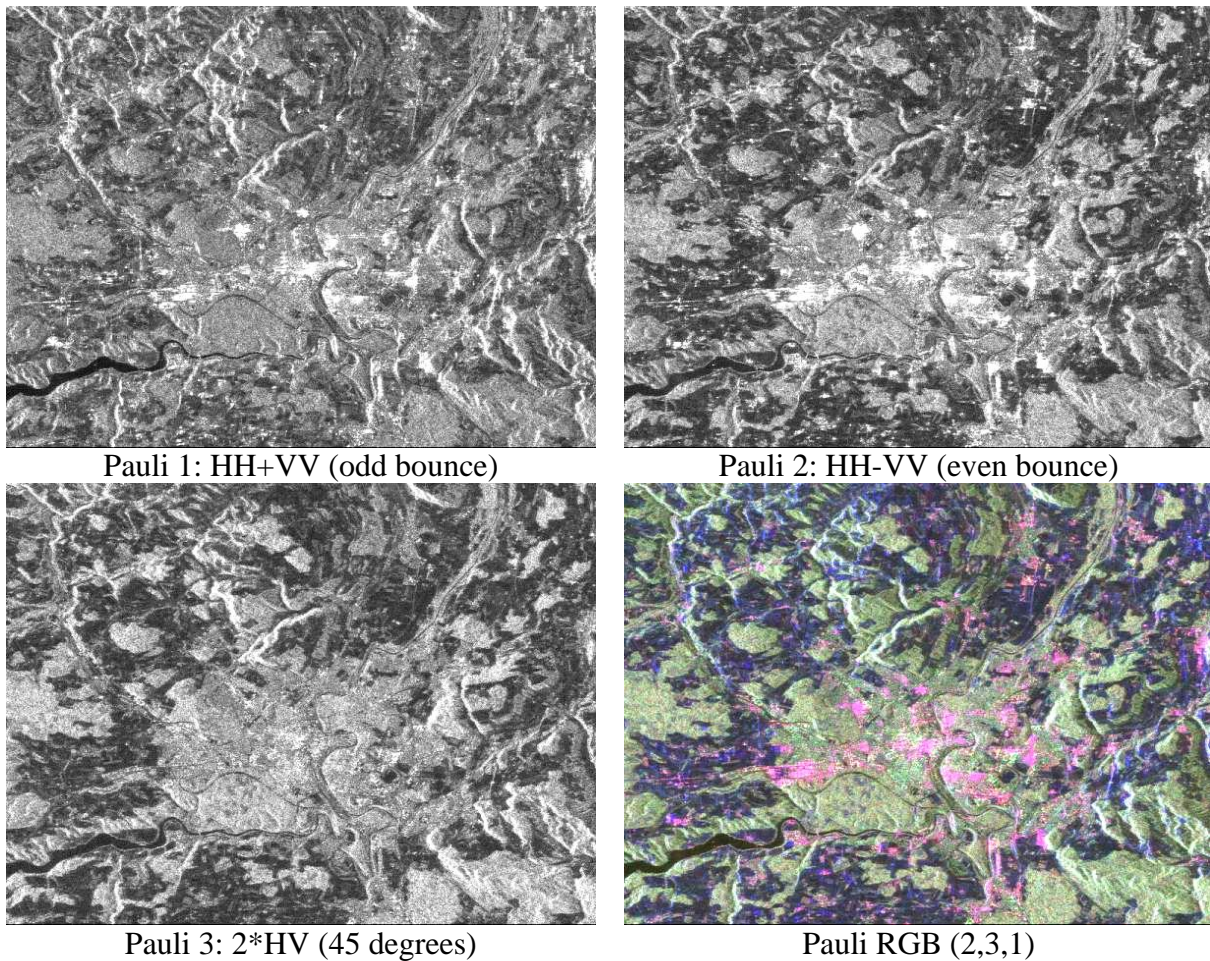
Pauli RGB (2,3,1)

Figure 4. Pauli components of original ALOS PALSAR dataset and RGB color composites.

The RGB can be displayed with the program ***disras*** (DISP module)

```
disras 20061020.pauli.rgb.ras
```

Figure 4 shows the three Pauli components and the RGB image. With respect to Figure 3 showing the lexicographic representation, the Pauli coding shows differences in the agricultural areas, which previously appeared all in purple, whereas here there are both purple and blue shades showing the gradient in the HH and VV channels, corresponding to different proportion of the odd and even bounce. Forest areas are characterized by strong 45 degrees component whereas even bounces and somewhat odd bounces are typical of urban areas.

Another form of representing polarimetric data in form of a RGB color composite consists in putting a co-pol intensity image in red (HH or VV), the cross-pol intensity image in green (HV) and the ratio between the co-pol and the cross-pol image in blue. This color composite is particularly useful in the case of dual-polarization data.

4. Polarimetric coherency and covariance matrix

Information about different scattering mechanisms can be evidenced by taking second order moments from the scattering matrix, **S**. This information is stored in the coherency and covariance matrices.

The coherency matrix, T_3, is a 3×3 matrix based on the Pauli vector representation:

$$T_3 = \left\langle \underline{k} \cdot \underline{k}^{*T} \right\rangle \tag{5}$$

resulting in products of the sum and difference of the co-pol components and the cross-pol component. The terms of the main diagonal are real-valued (T_{11}, T_{22}, T_{33}) and correspond to the intensities of the Pauli components. The remaining elements represent the correlation between the Pauli components. The generation of individual elements of the coherency matrix is supported by the program *polcoh.*

```
polcoh          20061020.pauli_alpha.slc          20061020.pauli_beta.slc
20061020.pauli_gamma.slc        20061020.hh.slc.par        20061020.hv.slc.par
20061020.vv.slc.par 20061020 20061020.coh.par 1 7
```

The output in this example will have file name "20061020" and extension equal to the position in the coherency matrix (e.g. t11, t12, t23). The elements of the main diagonal are all in floating point format. The off-diagonal elements are in FCOMPLEX format. A single parameter file for the output will be generated and stored as 20061020.coh.par. The elements of the coherency matrix are obtained according to multi-look factors specified by the user.

The covariance matrix, **C₃**, is a is a 3×3 matrix based on the lexicographic representation:

$$C_3 = \left\langle \underline{\Omega} \cdot \underline{\Omega}^{*T} \right\rangle \tag{6}$$

resulting in products of the elements of the scattering matrix **S**. The terms of the main diagonal are real-valued (C_{11}, C_{22}, C_{33}) and correspond to the intensities of the co-pol and cross-pol channels. The remaining terms express the correlation between two channels. The generation of individual elements of the coherency matrix is supported by the program *polcovar*. The output will have "20061020" as file name. The extension depends on the position within the covariance matrix (e.g. c11, c12, c23). Components of the diagonal are in floating point format. Off-diagonal components are in float-complex format. A single parameter file for the output will be generated and stored as 20061020.covar.par. The elements of the covariance matrix are obtained according to multi-look factors specified by the user.

```
polcovar        20061020.hh.slc        20061020.hv.slc        20061020.vv.slc
20061020.hh.slc.par    20061020.hv.slc.par    20061020.vv.slc.par    20061020
20061020.covar.par 1 7
```

5. Kennaugh matrix

While the scattering matrix describes as en ensemble the scattering from a target, a representation that separates different scattering mechanisms might be more useful to understand the properties of a scene. The Kennaugh matrix is a 4×4 matrix. The derivation of the matrix has been shown in several publications. For completeness it is referred to [1]. In total 9 parameters, the Huynen parameters, are obtained, representing symmetric, non-symmetric and coupled targets.

$$K_4 = \begin{bmatrix} A_0 + B_0 & C & H & F \\ C & A_0 + B & E & G \\ H & E & A_0 - B & D \\ F & G & D & -A_0 + B_0 \end{bmatrix}$$

where A_0, B_0, B, C, D, E, F, G and H are the nine Huynen parameters. If a target can be seen as a pure target, the scattering not being influenced by fluctuations during exposure or clutter, the coherency matrix can be written in terms of the Huynen parameters [1]:

$$T_3 = \begin{bmatrix} 2A_0 & C - jD & H + jG \\ C + jD & B_0 + B & E + jF \\ H - jG & E - jF & B_0 - B \end{bmatrix} \tag{7}$$

For an interpretation of the parameters it is referred to page 76 in [1].

The LAT module supports the computation of these parameters starting from the coherency matrix elements with the script **KENNAUGH_MATRIX**. Below we show an example for the generation of the first element of the matrix. The output will have a file name consisting of a common term (in this case "20061020") and an extension indicating the position within the matrix (e.g. k11, k12, k23 etc.)

```
./KENNAUGH_MATRIX   20061020.t11   20661020.t22   20061020.t33   20061020.t12
20061020.t13 20061020.t23 800 20061020 1
```

6. Change of polarization basis

The scattering matrix **S** is generally provided in the horizontal and vertical polarization components. It might be useful to apply a transformation of basis in order to highlight some scattering mechanisms that are not directly visible in the original linear polarization basis. The polarimetric basis change consists in transforming the original scattering matrix to a new elliptical polarization basis defined by the angles ψ (orientation), χ (ellipticity) that represent the polarization ellipse and α (relative phase).

6.1. Orthonormal polarization basis

The orthonormal polarization basis consists basically in a rotation of 45 degrees to obtain a linear polarization at 45° and the orthogonal polarization at -45°. In this case $\psi=45°$, $\chi=0°$ and α is assumed to be equal to 0. The scattering matrix in the linear polarization basis can be transformed to the orthogonal basis with the program ***lin_comb_cpx*** as follows:

S$_{AA}$, linear polarization at 45°

```
lin_comb_cpx 3 20061020.hh.slc 20061020.vv.slc 20061020.hv.slc 0 0 0.5 0
0.5 0 1 0 20061020.saa 800 - - 1 1 1
```

S$_{OO}$, perpendicular to S$_{AA}$

```
lin_comb_cpx 3 20061020.hh.slc 20061020.vv.slc 20061020.hv.slc 0 0 0.5 0
0.5 0 -1 0 20061020.soo 800 - - 1 1 1
```

S$_{AO}$, cross-polarized term

```
lin_comb_cpx  2  20061020.hh.slc  20061020.vv.slc  0  0  -0.5  0  -0.5  0
20061020.sao 800 - - 1 1 1
```

Visual representation can be helpful in the Pauli basis. Hence, first the three Pauli components need to be generated (see Section 3). The sequence of commands is shown below where the files *.pauli_ao indicate the Pauli components.

```
pauli    20061020.saa    20061020.soo    20061020.sao    20061020.hh.slc.par
20061020.vv.slc.par 20061020.hv.slc.par 20061020.pauli_ao
```

To generate the RGB with the GAMMA software, at first the SUNraster version of the three Pauli components must be generated. Since the data is in FCOMPLEX format and we are primarily interested in the magnitude, the program ***rasSLC*** (DISP module) is used. To decrease noise, multi-looking is applied with factors 1 and 7 (see Section 2).

```
rasSLC 20061020.pauli_ao_alpha.slc 800 - - 1 7
```

```
rasSLC 20061020.pauli_ao_beta.slc 800 - - 1 7
```

```
rasSLC 20061020.pauli_ao_gamma.slc 800 - - 1 7
```

With the program ***ras_to_rgb*** the RGB can be obtained.

```
ras_to_rgb  20061020.pauli_ao_beta.slc.ras  20061020.pauli_ao_gamma.slc.ras
20061020.pauli_ao_alpha.slc.ras 20061020.pauli_ao.rgb.ras
```

The RGB can be displayed with the program ***disras*** (DISP module)

```
disras 20061020.pauli_ao.rgb.ras
```

The RGB color composite is shown in Figure 5. The reddish color in correspondence of forests indicates a strong difference component. Most fields appear in blue corresponding to the sum of the two orthogonal components. With respect to the Pauli representation in Figure 3 in this case there is not a substantial increase in information obtained after the transformation of basis.
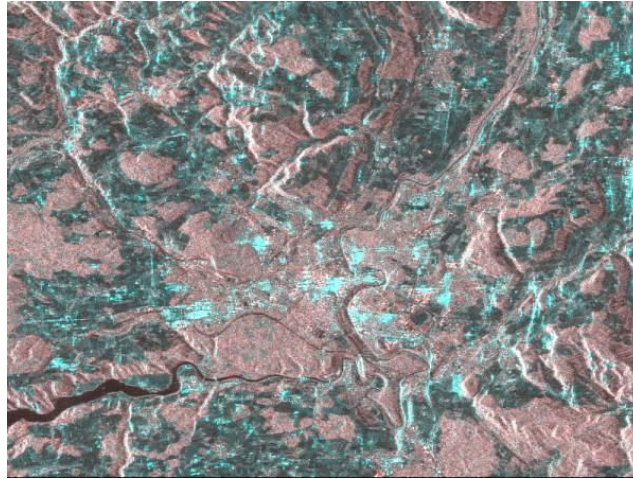
Figure 5. Pauli RGB for the scattering matrix in the orthogonal polarization basis.

6.2. Circular polarization basis

The transformation to the circular polarization basis corresponds in expressing the scattering matrix in terms of the left circular and right circular components [1]. While the orientation angle can be any value between -90° and +90°, the ellipticity angle is 45° is the case of left circular polarization basis and -45° in the case of right circular polarization basis. The change of polarization basis can be performed with the program ***lin_comb_cpx***. For the right-right (RR), left-left (LL) and right-left (RL) elements the command lines look as follows

$\# \; S_{rr} = iS_{hv} + (S_{hh} - S_{vv})/2$ (8)

```
lin_comb_cpx 3 20061020.hh.slc 20061020.vv.slc 20061020.hv.slc 0 0 0.5 0 -
0.5 0 0 1 20061020.rr 800 - - 1 1 1
```

$\# \; S_{ll} = iS_{hv} - (S_{hh} - S_{vv})/2$ (9)

```
lin_comb_cpx 3 20061020.vv.slc 20061020.hh.slc 20061020.hv.slc 0 0 0.5 0 -
0.5 0 0 1 20061020.ll 800 - - 1 1 1
```

$\# \; S_{rl} = i \; (S_{hh} + S_{vv})/2$ (10)

```
lin_comb_cpx 2 20061020.hh.slc 20061020.vv.slc 0 0 0 0.5 0 0.5 20061020.rl
800 - - 1 1 1
```

A color composite using the Pauli RGB system can be obtained as follows (sum, difference, cross-term) as already shown in the previous Section. The result is displayed in Figure 6.

```
pauli    20061020.rr    20061020.ll    20061020.rl    20061020.hh.slc.par
20061020.vv.slc.par 20061020.hv.slc.par 20061020.pauli_lr

rasSLC 20061020.pauli_lr_alpha.slc 800 - - 1 7

rasSLC 20061020.pauli_lr_beta.slc 800 - - 1 7

rasSLC 20061020.pauli_lr_gamma.slc 800 - - 1 7
```

```
ras_to_rgb   20061020.pauli_lr_beta.slc.ras   20061020.pauli_lr_gamma.slc.ras
20061020.pauli_lr_alpha.slc.ras 20061020.pauli_lr.rgb.ras

disras 20061020.pauli_lr.rgb.ras
```
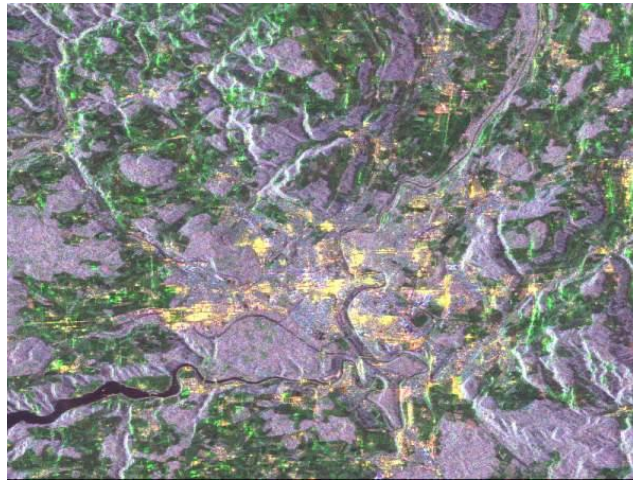

Figure 6. Pauli RGB for the scattering matrix in the circular polarization basis.

Figure 6 shows that the forests appear in purple, thus meaning that they are characterized by a strong first and second component in the Pauli sense indicating strong co-pol term in the right and the left circular polarizations. Bare soils are instead characterized by the third Pauli component as they appear primarily in green, this meaning that the right-left component is strongest. Urban areas appear in yellow meaning strong second and third component.

7. Polarimetric target decomposition

Target decomposition is an effective approach to reconstruct the scattering mechanisms in the scattering matrix into a different representation to obtain a new set of components directly related to some scattering mechanisms specific of individual targets. Different approaches for the so called target decomposition have been proposed in the literature. Here we will apply some selected decompositions, namely the Huynen, Cloude, Freeman-Durden, Krogager, and Cloude-Pottier decomposition.

7.1. Huynen decomposition

In Section 5 it was shown that the Kennaugh matrix summarizes all sort of scattering possibilities. The Huynen decomposition separates the coherency matrix into two parts, one being related to an "equivalent single target" and one related to a residual target in order to synthesize the same scattering mechanisms represented in the Kennaugh matrix but for an effective single target. In particular, with this decomposition, the non-symmetrical terms (B_0, B, E and F) are written in terms of a single-target term and a non-symmetric target called N-target.

$$B_0 = B_{0T} + B_{0N}$$

$$B = B_T + B_N$$
$$E = E_T + E_N \quad\quad\quad (11)$$
$$F = F_T + F_N$$

In other words the coherency matrix T_3 can be written as a sum of a coherency matrix related to the equivalent single target, T_0, and the coherency matrix of the N-target, T_N.

The Huynen decomposition is supported by the LAT script ***HUYNEN_DEC***. With this script the equivalent single target components of the scattering matrix T_{0_22}, T_{0_33} and T_{0_23} can be obtained. The other elements of the coherency matrix do not change. Below an example to compute the component T_{0_22}, The output will be called 20061020.t22_0

```
./HUYNEN_DEC 20061020.hh.slc 20061020.hv.slc 20061020.vv.slc 20061020.t11
20061020.t12 20061020.t13 800 20061020 1
```

7.2. Cloude decomposition

In [2] it was shown that with an eigenvector decomposition of the coherency matrix it is possible to obtain information directly related to the dominant scattering mechanism of a target by looking at the largest eigenvalue. The target vector obtained with this decomposition is:

$$\underline{k} = e^{j\phi} \begin{bmatrix} \sqrt{2A_0} \\ \sqrt{B_0 + B}\, e^{+j\tan^{-1}(D/C)} \\ \sqrt{B_0 - B}\, e^{-j\tan^{-1}(G/H)} \end{bmatrix} \quad\quad\quad (12)$$

Each of the target generators is related to a specific scattering mechanism. If the magnitude of the first target generator is greater than the other two, the target is characterized by surface scattering. If the magnitude of the second target generator is greater than the other two, the target is characterized by dihedral scattering. Finally, if the magnitude of the third target generator is greater than the first and the second components, the scattering is primarily volume scattering.

The generation of the target vector components is supported by the LAT script ***CLOUDE_DEC***, which requires the scattering matrix, the T_{12} and T_{13} elements of the coherency matrix. Multi-look factors of 1 and 7 are applied to reduce noise.

```
./CLOUDE_DEC 20061020.hh.slc 20061020.hv.slc 20061020.vv.slc 20061020.t12
20061020.t13 800 20061020 1 7
```

The output consists of three images of magnitude and two images of the phase (for the second and third component). The result can be displayed by means of a RGB color composite. At first SUNraster images of the individual magnitude images need to be generated for example with the DISP program ***raspwr***. Alternatively ***ras_dB*** or ***ras_linear*** can be used.

```
raspwr 20061020.ctd_1.mag 800
```

```
raspwr 20061020.ctd_2.mag 800
```

```
raspwr 20061020.ctd_3.mag 800
```

The RGB (Pauli color coding) is generated with the program ***ras_to_rgb*** as follows

```
ras_to_rgb        20061020.ctd_2.mag.ras        20061020.ctd_3.mag.ras
20061020.ctd_1.mag.ras 20061020.ctd.rgb.ras
```

The image can be displayed with the DISP program ***disras.***

```
disras 20061020.ctd.rgb.ras
```
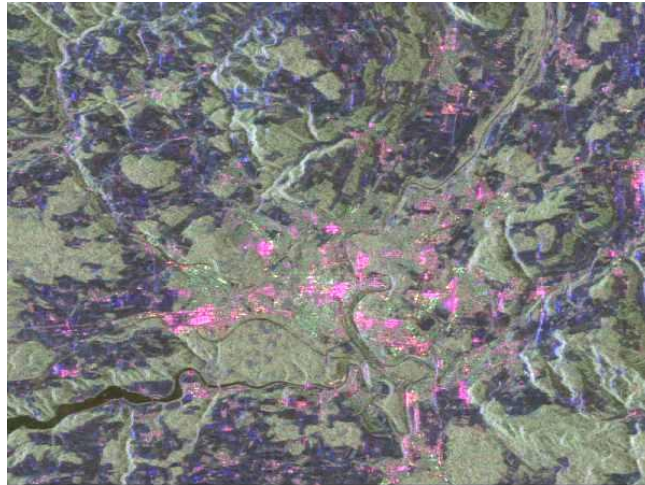

Figure 7. RGB of the Cloude target vector (R: 2ⁿᵈ component, G: 3ʳᵈ component, B: 1ˢᵗ component).

Figure 7 shows the RGB using the Pauli color coding. Areas appearing as green are characterized by a strong third component, thus meaning that volume scattering is the dominant mechanism in these areas. This is consistent with the fact that these areas correspond to forests. Areas appearing as blue are characterized by a strong first component, which is related to surface scattering. These are predominantly bare fields. Urban areas appear instead mostly as pink, which mean strong first and second component, this meaning that both surface and dihedral scattering are dominant.

7.3. Freeman-Durden decomposition, 3 components

For natural scatterers (forest, cropland, bare soil) Freeman and Durden proposed a decomposition into main scattering mechanisms (surface scattering, double-bounce and volume scattering), which enables the possibility to distinguish between different land cover types without the need of reference data.

The model-based decomposition of the scattering matrix links the individual components to the surface, double-bounce and volume contribution to the total backscatter. The surface and double-bounce contributions, f_s and f_d, are related to the co-polarized elements of the scattering matrix as follows. In (13) α and β represent the first term in the third equation for 100% double-bounce and surface scattering respectively. The estimation of the four (unknown) parameters from the scattering matrix elements is described in [3].

$$\left\langle \left| S_{hh} \right|^2 \right\rangle = f_s \left| \beta \right|^2 + f_d \left| \alpha \right|^2$$
$$\left\langle \left| S_{vv} \right|^2 \right\rangle = f_s + f_d \qquad\qquad (13)$$
$$\left\langle S_{hh} S_{vv}^{*} \right\rangle = f_s \beta + f_d \alpha$$

The volume term, f_v, is instead expressed as

$$P_v = 8 f_v / 3 \qquad\qquad (14)$$

with P_v being the part of the span due to volume scattering

$$P = P_s + P_d + P_v \qquad\qquad (15)$$

In (15) P_s and P_d are linked to the four unknown parameters in (13) by means of:

$$P_s = f_s \left(1 + \left| \beta \right|^2 \right) \qquad\qquad (16)$$
$$P_d = f_d \left(1 + \left| \alpha \right|^2 \right) \qquad\qquad (17)$$

The Freeman-Durden three-component target decomposition is supported by the LAT script **FD3C_DEC**. Multi-look factors of 1 and 7 are applied to reduce noise.

```
./FD3C_DEC 20061020.hh.slc 20061020.hv.slc 20061020.vv.slc 20061020.t13 800
20061020 1 7
```

The input consists of the 3 images forming the scattering matrix and the T_{13} element of the coherency matrix. The output will consist of three files with common file name "20061020" and extension "fdd_ps", "fdd_pd" and "fdd_pv" representing respectively the power component of surface, double-bounce and volume scattering.

For visual interpretation a RGB of three components can be generated. At first a SUNraster image needs to be generated for each power image. This is done here with the program **raspwr**. Alternatively, the programs **ras_dB** or **ras_linear** can be used.

```
raspwr 20061020.fdd_ps 800

raspwr 20061020.fdd_pd 800

raspwr 20061020.fdd_pv 800
```

With the program **ras_to_rgb** the RGB can be obtained. The order is such that the double-bounce, volume and surface components are put in red, green and blue respectively.

```
ras_to_rgb  20061020.fdd_pd.ras  20061020.fdd_pv.ras  20061020.fdd_ps.ras
20061020.fdd.rgb.ras
```

The output can be displayed with the program **disras**:

```
disras 20061020.fdd.rgb.ras
```

Figure 8 shows the RGB color composite highlighting in green areas where volume scattering is predominant (forest), in blue areas of dominant surface scattering (bare fields) and in red areas with dominant double-bounce. Urban areas present a mixture of double-bounce and surface scattering.
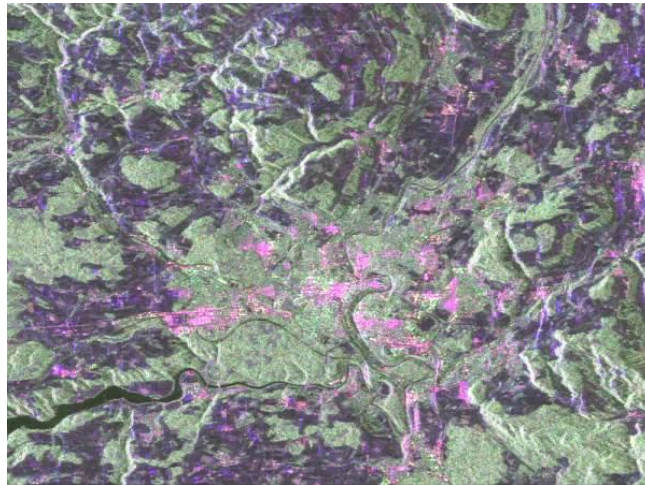
Figure 8. RGB of Freeman-Durden three-component decomposition (R: double-bounce, G: volume, B: surface scattering).

7.4. Krogager decomposition

In [4] a roll invariant decomposition interpretation was introduced where the actual scattering matrix can be regarded as a superposition of the basic scattering mechanisms isotropic surface, diplane and helix. It can be derived from the circular scattering components S_{rr}, S_{ll}, S_{rl} (see Section 6.2).

The surface scattering component Sphere is

$$\text{Sphere} = |S_{rl}| \tag{18}$$

The Diplane and Helix components are defined as:

$$\text{if } |S_{rr}| > |S_{ll}|: \text{ Diplane} = |S_{rr}| \text{ and Helix} = |S_{rr}| - |S_{ll}| \tag{19}$$

$$\text{if } |S_{rr}| < |S_{ll}|: \text{ Diplane} = |S_{ll}| \text{ and Helix} = |S_{ll}| - |S_{rr}| \tag{20}$$

The circular scattering components has been obtained in Section 6.2. To reduce noise, simple multi-looking can be applied.

```
multi_look 20061020.rl 20061020.hh.slc.par 20061020.sphere 20061020.mli.par
1 7
```

The other two components are used as input by the program ***diplane_helix*** to compute the diplane and helix components.

```
diplane_helix 20061020.ll 20061020.rr 20061020.hh.slc.par 20061020.diplane
20061020.helix 20061020.mli.par 1 7 - - -
```

The sphere, deplane and helix components can be combined in a RGB image product by first generating the SUNraster images (for example with ***raspwr***) and then by combining them with the DISP program ***ras_to_rgb***.

```
raspwr 20061020.sphere 800

raspwr 20061020.diplane 800

raspwr 20061020.helix 800

ras_to_rgb   20061020.diplane.ras   20061020.helix.ras   20061020.sphere.ras
20061020.sdh.rgb.ras
```
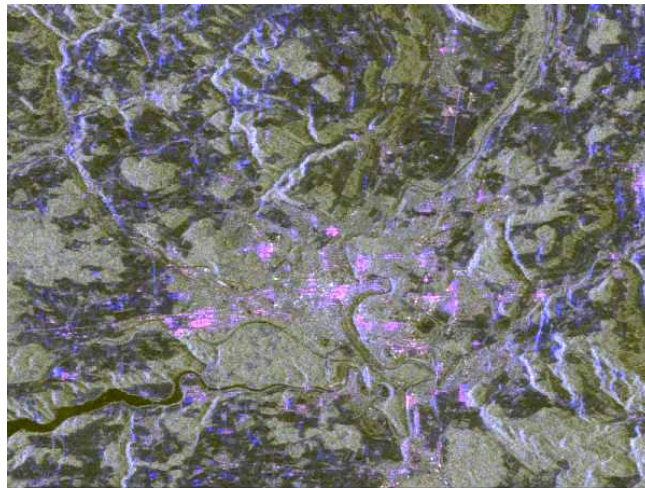

Figure 9. Sphere (blue), diplane (red) and helix (green) RGB color composite.

The output can be displayed with the DISP program ***disras***. Figure 9 shows the colour composite of the sphere, diplane and helix components of the ALOS PALSAR dataset. Forested areas appear as a mixture of all scattering mechanisms while some fields show either plane or helix scattering characteristics. Urban areas show diplane and partly sphere characteristics.

7.5. Cloude and Pottier decomposition

For remote sensing applications the assumption of deterministic scatterers is usually not valid, since the resolution is bigger than the wavelength. Especially vegetated areas contain many spatially distributed scatterers. The measured scattering matrix of a given resolution cell consists of the coherent integration of all scatterers. To deal with statistical scattering effects and the analysis of extended scatterers the Cloude and Pottier decomposition theorem is straightforward and is capable of covering a range of scattering mechanisms. It is based on the eigenvector analysis of the coherence matrix **T**.

The coherence matrix **T** is a Hermitian semi definite matrix. That means it has real valued eigenvalues λ.

$$\mathbf{T}\omega = \lambda\omega \tag{21}$$

Thus the matrix **T** can be decomposed in 3 matrices $\mathbf{T}_n$ that are given by the corresponding eigenvectors ω and eigenvalues λ.

$$\mathbf{T} = \sum_{n=1}^{3} \lambda_n \mathbf{T}_n = \lambda_1 \left(\omega_1 \omega_1^H \right) + \lambda_2 \left(\omega_2 \omega_2^H \right) + \lambda_3 \left(\omega_3 \omega_3^H \right) \tag{22}$$

Each matrix $\mathbf{T}_n$ is a unitary scattering matrix representing a deterministic scattering contribution weighted by the eigenvalues λ_n. Two important physical features arise from this decomposition, the entropy H, introduced by [5], and the anisotropy A, introduced by [6].

The polarimetric scattering entropy H is a measure of the distribution of the components of the scattering process and is $0 <= H <= 1$

$$H = -P_1 \log_3 P_1 - P_2 \log_3 P_2 - P_3 \log_3 P_3$$

$$P_i = \frac{\lambda_i}{\sum_{j=1}^{3} \lambda_j} \tag{23}$$

If H=0 then **T** has only one eigenvector and it represents a deterministic scattering process. If H=1 it means that $\lambda_1 = \lambda_2 = \lambda_3$.

While H contains mainly information between λ_1 and the two other eigenvalues, the polarimetric anisotropy A depends on the difference between the latter

$$A = \frac{\lambda_2 - \lambda_3}{\lambda_2 + \lambda_3} \tag{24}$$

For high entropy the anisotropy gives no additional information because the eigenvalues are almost equal. If the entropy is medium or low the anisotropy delivers additional information about the scattering process. From the eigenvectors the α–angles can be determined which are related to the type of scattering.

$$\omega_i = \begin{bmatrix} \cos\alpha_i e^{i\phi_i} \\ \sin\alpha_i \cos\beta_i e^{i\delta_i} \\ \sin\alpha_i \cos\beta_i e^{i\gamma_i} \end{bmatrix} \tag{25}$$

The interpretation of the angles is given in [7].
α: target scattering type 0° .. 90°
β: orientation of target -180° .. 180°
ϕ,δ,γ: target phase angles

The α–angle is an averaged value and denotes a mean scattering mechanism and can be derived from

$$\alpha = \sum_{i=1}^{3} P_i \alpha_i \tag{26}$$

The resulting α–angle can be misleading if different scattering mechanisms are present in the same resolution cell!
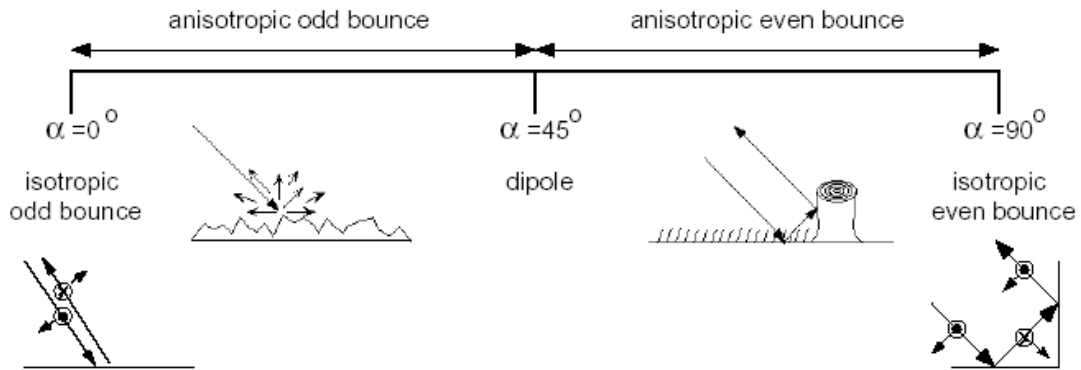
Figure 10. Interpretation of the α-angle values. The main parameter for identifying the dominant scattering mechanism is α. This angle has a useful range of 90 and corresponds to a continuous change from surface scattering in the geometrical optics (GO) limit (α =0°) through surface scattering under physical optics (PO) to the Bragg surface model, encompassing dipole scattering and moving into double bounce scattering mechanisms between two dielectric surfaces, finally reaching dihedral scatter from metallic surfaces at α=90°.

In [5] the authors proposed a classification based on the situation of a target in the H-α plane as shown in Figure 11. All random scattering mechanisms can be represented in this space. However, not all regions are equally populated. For example, when H=1 there is only one possible value for alpha, α=60°. This reflects the increasing inability to distinguish between scattering mechanisms as the underlying entropy increases. On the other hand at H=0 the full range of possible alpha values is possible. We can quantify the variation in this feasible region of points by the black lines in Figure 11, determined by the H-α variation for a coherency matrix with degenerate minor eigenvalues with amplitude m (0<=m<=1).

$$\mathbf{T}_I = \begin{bmatrix} 1 & 0 & 0 \\ 0 & m & 0 \\ 0 & 0 & m \end{bmatrix}; \ 0 \leq m \leq 1 \tag{2}$$

$$\mathbf{T}_{II} = \begin{bmatrix} 0 & 0 & 0 \\ 0 & 1 & 0 \\ 0 & 0 & 2m \end{bmatrix}; \ 0 \leq m \leq 0.5 \tag{3}$$

$$\mathbf{T}_{II} = \begin{bmatrix} 2m-1 & 0 & 0 \\ 0 & 1 & 0 \\ 0 & 0 & 1 \end{bmatrix}; \ 0.5 \leq m \leq 1 \tag{4}$$

Alpha - Entropy Distribution
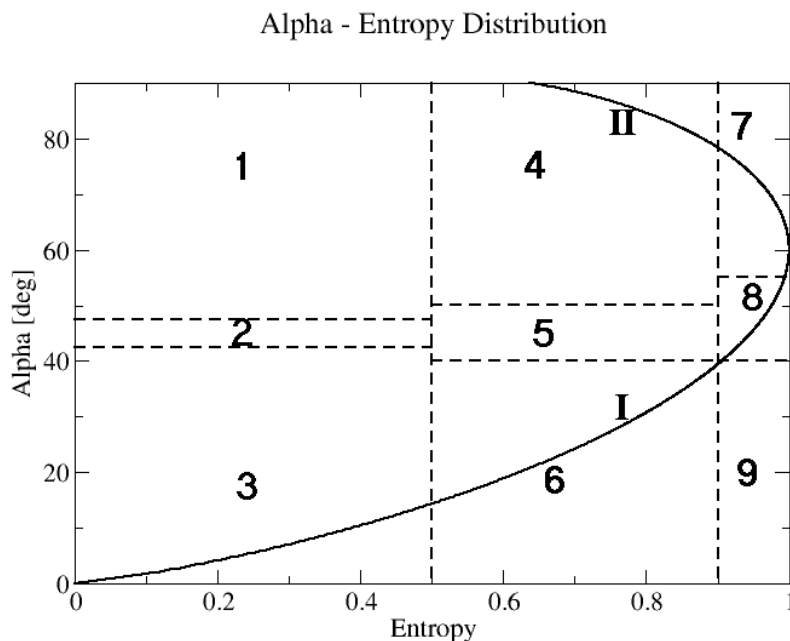
Figure 11. Alpha-Entropy classification scheme.

The H-α plane is subdivided into 9 areas with distinct scattering mechanisms (Figure 11):

Zone 1: Low Entropy Multiple Scattering Events
This zone corresponds to low entropy double or 'even' bounce scattering events, such as provided by isolated dielectric and metallic dihedral scatterers. These are characterized by α>47.5°. The lower bound chosen for this zone is dictated by the expected dielectric constant of the dihedrals and by the measurement accuracy of the Radar. The upper entropy boundary for these first three zones is chosen on the basis of tolerance to perturbations of first order scattering theories (which generally yield zero entropy for all scattering processes). By estimating the level of entropy change due to second and higher order events, tolerance can be built into the classifier so that the important first order process can still be correctly identified. Note also that system measurement noise will act to increase the entropy and so the system noise floor should also be used to set the boundary. H = 0.5 is chosen as a typical value accounting for these two effects.

Zone 2: Low Entropy Dipole Scattering
In this zone occur strongly correlated mechanisms which have a large imbalance between hh and vv in amplitude. An isolated dipole scatterer would appear here, as would scattering from vegetation with strongly correlated orientation of anisotropic scattering elements.

Zone 3: Low Entropy Surface Scatter
In this zone occur low entropy scattering processes with alpha values less than 42.5°. These include GO and PO surface scattering, Bragg surface scattering and specular scattering phenomena which do not involve 180° phase inversions between hh and vv. Physical surfaces such as water at L and P-Bands, sea-ice at L-Band, as well as very smooth land surfaces, all fall into this category.

Zone 4: Medium Entropy Multiple Scattering

This zone accounts for dihedral scattering with moderate entropy. This occurs for example in forestry applications, where double bounce mechanisms occur at P and L bands following propagation through a canopy. The effect of the canopy is to increase the entropy of the scattering process. A second important process in this category is urban areas, where dense packing of localized scattering centers can generate moderate entropy with low order multiple scattering dominant. The boundary between zones 4, 5, 6 and 7, 8, 9 is set as 0.9. This is chosen on the basis of the upper limit for surface, volume and dihedral scattering before random distributions apply.

Zone 5: Medium Entropy Vegetation Scattering
Here again we have moderate entropy but with a dominant dipole type scattering mechanism. The increased entropy is due to a central statistical distribution of orientation angle. Such a zone would include scattering from vegetated surfaces with anisotropic scatterers and moderate correlation of scatterer orientations.

Zone 6: Medium Entropy Surface Scatter
This zone reflects the increase in entropy due to changes in surface roughness and due to canopy propagation effects. In surface scattering theory the entropy of low frequency theories like Bragg scatter is zero. Likewise, the entropy of high frequency theories like Geometrical Optics is also zero. However, in between these two extremes, there is an increase in entropy due to the physics of secondary wave propagation and scattering mechanisms. Thus as the roughness/correlation length of a surface changes, its entropy will increase. Further, a surface cover comprising oblate spheroidal scatterers (leafs or discs for example) will generate an entropy between 0.6 and 0.7. We set a bound of $H = 0.9$ as an upper limit for these changes.

Zone 7: High Entropy Multiple Scattering
We can still distinguish double bounce mechanisms in a high entropy environment. Such mechanisms can be observed in forestry applications or in scattering from vegetation which has a well developed branch and crown structure.

Zone 8: High Entropy Vegetation Scattering
High entropy volume scattering arises when $\alpha=45°$ and $H =0.95$. This can arise for single scattering from a cloud of anisotropic needle like particles or from multiple scattering from a cloud of low loss symmetric particles. In both cases however, the entropy lies above 0.9, where the feasible region of H-α space is rapidly shrinking. Scattering from forest canopies lies in this region, as does the scattering from some types of vegetated surfaces with random highly anisotropic scattering elements. The extreme behavior in this class is random noise i.e., no polarization dependence, a point which lies to the extreme right of Figure.

Zone 9: High Entropy Surface Scatter
This class is not part of the feasible region in H-α space i.e., we cannot distinguish surface scattering with entropy H>0.9. This is a direct consequence of our increasing inability to classify scattering types with increasing entropy.

The decomposition of the scattering matrix into entropy, anisotropy and alpha is supported by the program **haalpha**.

```
haalpha          20061020.pauli_alpha.slc          20061020.pauli_beta.slc
20061020.pauli_gamma.slc       20061020.hh.slc.par          20061020.cpd_A
20061020.cpd_alfa    20061020.cpd_H    20061020.cpd_l1    20061020.cpd_l2
20061020.cpd_l3 20061020.mli.par 1 7
```

In this command line the input corresponds to the three Pauli components of the scattering matrix, which can be computed as described in Section 3. The output consists of the three images of H, A and α and the three eigenvalues. The extension "cpd" has been used to indicate that all outputs refer to the Cloude and Pottier decomposition.

The H, A and α components can be displayed with the program ***dis_linear*** using as intervals for display the values 0 and 1 for H and A, and the values 0 and 90 for α.

```
dis_linear 20061020.cpd_H 800 - - 0 1

dis_linear 20061020.cpd_A 800 - - 0 1

dis_linear 20061020.cpd_alfa 800 - - 0 90
```

Figure 12 shows the three components. The entropy is particularly high in correspondence of the forest areas and water surfaces. Anisotropy is highest in correspondence of urban areas. The α angle shows higher values in correspondence of forest and urban areas. The interpretation of the signatures follows from the diagram in Figure 11.
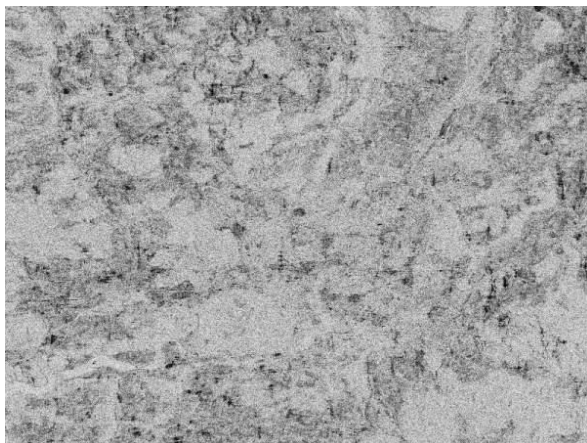
H, entropy

A, anisotropy

α
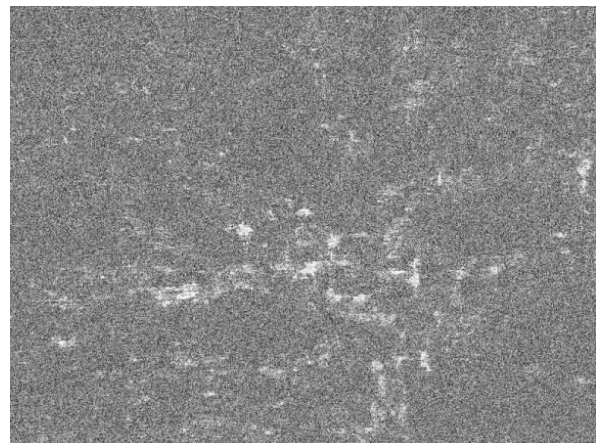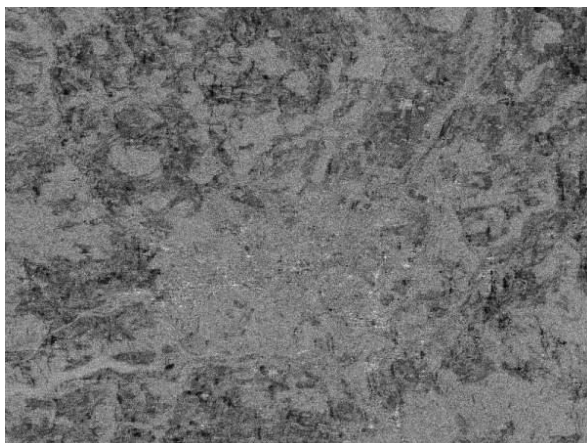
Figure 13. Entropy, anisotropy and α images for the ALOS PALSAR dataset in Figure 1.

8. References

[1] J.-S. Lee and E. Pottier, *Polarimetric radar imaging: from basics to applications*. Boca Raton: CRC Press, 2009.

[2] S. R. Cloude and E. Pottier, "A review of target decomposition theorems in radar polarimetry," *IEEE Transactions on Geoscience and Remote Sensing*, vol. 34, pp. 498-518, 1996.

[3] A. Freeman and S. L. Durden, "A three-component scattering model for polarimetric SAR data," *IEEE Transactions on Geoscience and Remote Sensing*, vol. 36, pp. 963-973, 1998.

[4] E. Krogager, "A new decomposition of the radar target scattering matrix," *Electronic Letters*, vol. 26, pp. 1525-1526, 1990.

[5] S. R. Cloude and E. Pottier, "An entropy based classification scheme for land applications of polarimetric SAR," *IEEE Transactions on Geoscience and Remote Sensing*, vol. 35, pp. 68-78, 1997.

[6] E. Pottier, "The H/A/alpha polarimetric decomposition approach applied to PolSAR data proceeding," *Proc. PIERS, Report EUR 18662 EN*, Italy, 1998.

[7] S. R. Cloude and E. Pottier, "Concept of polarisation entropy in optical scattering," *Optical Engineering*, vol. 34, pp. 1599-1610, 1995.